

# Arsenic- and metal-induced GaAs interface states by low-energy cathodoluminescence spectroscopy

R. E. Viturro, J. L. Shaw, and L. J. Brillson  
*Xerox Webster Research Center, Webster, New York 14580*

J. M. Woodall, P. D. Kirchner, G. D. Pettit, and S. L. Wright  
*IBM Thomas J. Watson Research Center, Yorktown Heights, New York 10598*

(Received 2 February 1988; accepted 4 May 1988)

We used optical emission techniques to obtain a direct measure of discrete electronic states at GaAs interfaces. These states depend on surface preparation, metallization, and semiconductor material. The energy of the discrete states found at metal/molecular-beam epitaxially grown GaAs(100) interfaces integrated within a Schottky formalism provides self-consistent results for the interface electrostatics. The presence of a large concentration of extrinsic defects causes the pinning behavior observed at metal/melt-grown GaAs(110) interfaces. These results provide the first direct experimental evidence for the origin of Fermi level "pinning" at metal/melt-grown GaAs junctions.

## I. INTRODUCTION

The identification of interface states and their role in Schottky barrier formation have long been key issues in the understanding of electronic properties of metal-semiconductor junctions.<sup>1-3</sup> We have used the low-energy cathodoluminescence spectroscopy (CLS) technique<sup>4-6</sup> to monitor the emission from surface and interface states formed during each stage of the surface preparation, metallization, and contact rectification. CLS provides direct information of metal-induced interface states which evolve in energy and density with multilayer metal coverages of the particular metal, extrinsic surface states due to lattice disruption, as well as bulk defect levels—all of which play a role in Schottky barrier formation.<sup>1-3</sup> Here we present CL and PL spectroscopy studies of bulk deep levels and of interface states at (110) UHV-cleaned melt-grown GaAs and at UHV-cleaned, ordered, molecular-beam epitaxially (MBE)-grown GaAs(100) interfaces with a variety of metals. These experiments reveal a number of distinct interface state features which depend on the surface preparation, the specific metallization as well as the quality of the semiconductor material. Such features correlate strongly with the observed differences in Fermi level ( $E_f$ ) stabilization for these different surfaces, interfaces, and bulk material.

## II. EXPERIMENT

The room temperature CL and PL measurements were carried out in an UHV chamber (base pressure =  $5 \times 10^{-11}$  Torr). The CLS excitation was produced by a chopped electron beam from a glancing incidence electron gun impinging on the specimen surface. The electron beam energy can be varied between 500–3500 eV to change the depth of electron excitation. This variability allows us to determine the interface specific features of the luminescence spectrum, otherwise difficult to identify because of the relatively large optical emission from GaAs bulk deep-level radiative recombination.<sup>4-7</sup> The values of the maximum steady-state excess carrier concentrations at the near surface region and

quantitative analysis of excitation depth have been published elsewhere.<sup>6,7</sup> PL excitation was produced by a HeNe laser (power = 6 mW, photon energy = 1.96 eV, excitation depth  $\sim 0.25 \mu\text{m}$ ) and by a HeCd laser (power = 10 mW, photon energy = 2.8 eV, excitation depth  $\sim 0.07 \mu\text{m}$ ). The luminescence was focused into a monochromator and the transmitted signal was phase detected by means of a liquid nitrogen ( $\text{LN}_2$ ) cooled Ge detector (North Coast,  $D^* = 5 \times 10^{14} \text{ cm Hz}^{-1/2} \text{ W}^{-1}$ ) and a lock-in amplifier. The response of the optical system was deconvolved by comparison of a black body spectrum with the measured spectrum of a W filament.

Measurements were carried out on both melt-grown and MBE-grown GaAs. Clean (110) GaAs surfaces (Crystal Specialties,  $n = 4 \times 10^{15} \text{ cm}^{-3}$ ) were obtained by cleaving (110) oriented bars in UHV. The quality of the cleaved surface was tested both visually, i.e., absence of laser light scattering from the surface, and by comparing the intensity ratio of the NBG transition to deep-level radiative recombination from PL and CL. For well-cleaved (110) (nonpolar) surfaces, constant PL/CL near band-gap (NBG) intensity ratios suggested that little or no band bending was present. Therefore, optical emission spectroscopic features are independent of excitation depth. Clean ordered MBE-grown GaAs(100) surfaces (Si-doped,  $n = 2-5 \times 10^{16} \text{ cm}^{-3}$ ) were obtained by thermal desorption of the As protective cap in UHV.<sup>8</sup> Thermal desorption spectroscopy (TDS) experiments were performed by raising the specimen temperature linearly in time and following the evolution of As with a UTI 100 °C mass spectrometer. Typical heating rates were in the range 2–10 °C/s. Additional pumping during the TDS experiments was provided by a 1000 l/s cryopump. Step desorption of the As cap was carried out by halting the thermal ramp at predetermined temperatures and annealing the specimen for 10 s. CLS, PLS, and Auger measurements were performed after each step. GaAs(100) is a polar surface which presents different reconstructions according to the particular surface stoichiometry. SXPS shows that the initial  $E_f$  position for the As-decapped GaAs(100) specimens are

in the range 0.55–0.8 eV. Thus the bands are bent and the optical emission spectrum is dependent on excitation depth with respect to the surface space charge region. We use the valence band (VB) spectra and the low-energy electron diffraction (LEED) pattern as criteria for high-quality, clean, ordered GaAs(100) surfaces. The surface stoichiometry and reconstruction of the GaAs(100) surfaces obtained by As decapping show a strong dependence on the desorption temperature. Reproducible CL and PL spectra were obtained in different runs.

We have used difference spectra in order to compare interface specific CL spectral features for different metal thicknesses on GaAs. The subtraction was carried out after normalizing the luminescence intensity with respect to dominant bulk deep level transition features always present in CL of GaAs.

Metals were evaporated from pre-outgassed W baskets onto the clean surfaces. Film thicknesses were monitored by means of a quartz crystal oscillator positioned next to the specimen surface. Monochromator scan energies, signal acquisition, rate of heating, and mass spectrometer were controlled by a microcomputer.

### III. RESULTS

#### A. As-related interface states

Figure 1 depicts the CLS spectra of As-capped MBE-grown and UHV-cleaned GaAs(100). The bottom CL spectrum of As/MBE-GaAs(100) specimen ( $n = 5 \times 10^{16} \text{ cm}^{-3}$ ) was obtained by heating the as-received sample to 380 °C for 5 s. The Auger spectrum shows that only As is present at the surface, with no indication of Ga or any contaminants. This procedure sublimes most of the As cap, usually several thousand Å, and leaves the GaAs(100) surface

with several layers of adsorbed As. The spectrum shows a near band gap (NBG) transition at 1.43 eV, plus a broad band with maximum at about 1.0 eV, a shoulder at 0.8 eV, and emission that extends to 1.3 eV. The clean spectrum of the MBE-grown GaAs was obtained after heating the specimen for 10 s at 570 °C. It shows an increase of the NBG transition intensity by a factor of 50, and a narrowing of the broadband at both sides of the peak maximum. The increase in NBG transition intensity can result from a decrease in both band bending and surface recombination velocity (SRV). Depth-resolved CLS and PLS confirm this decrease: excitation beyond versus within the surface space charge region exhibit only a modest increase in NBG emission for the clean surface as compared with a large increase for the As-capped surface. Reduction in surface recombination velocity (SRV), i.e., nonradiative carrier recombination mechanisms, may be related to the clean, ordered surface obtained after As decapping, as evidenced by VB spectra and the LEED pattern, respectively. The relatively weak peak feature remaining at 1.0 eV corresponds to deep traps residing in bulk GaAs, as confirmed by PLS. The intensity of this deep level emission varies within a small factor among different MBE-grown specimens. Clearly, the desorption of excess As from the GaAs(100) surface reduces band bending and SRV by suppressing interface states that are As related.

In order to study in detail the As-decapping procedure, we have performed TDS experiments of As coated MBE-grown GaAs(100). Figure 2 depicts the thermal desorption spectra of As, based on  $\text{As}^+$  (amu 75), for different heating rates. The temperature of the peak maxima shift to higher temperature and the peak intensity increases with increasing heating rate, as predicted for a simple desorption kinetic model including a finite pumping speed and linear heating rate. Three main desorption peaks are observed. The first desorption peak at about 400 °C corresponds to the sublimation of bulk As from the cap. Most likely the desorbing species is molecular  $\text{As}_4$ . The intensity of this peak appears

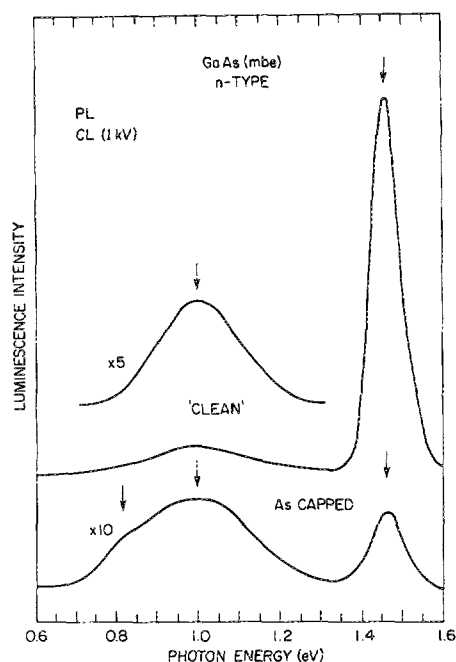


FIG. 1. CL spectra of As-capped MBE-grown and UHV-cleaned GaAs(100).

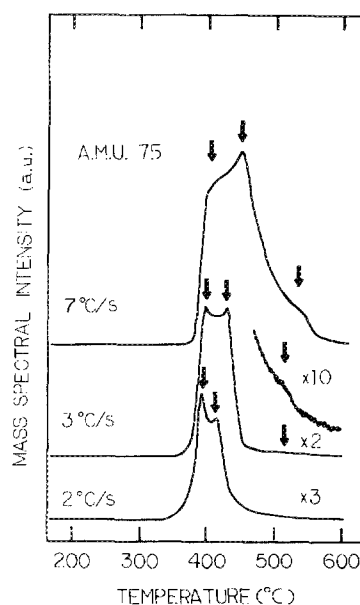


FIG. 2. Thermal desorption spectra of As/MBE-grown GaAs(100) for different heating rates.

small when compared with the other two desorption peaks because the TD spectrum of amu 75, represents only the fraction of  $\text{As}^+$  from the cracking pattern of desorbed molecular  $\text{As}_4$ . The total pressure measurements carried out simultaneously with the mass spectrum showed a large pressure increase which peaks at about 400 °C. The second and third desorption peaks correspond to additional desorption of As from GaAs(100) surface. We do not know yet which are the corresponding desorption species, but the relatively high intensity of the peaks suggests the desorption of  $\text{As}_2$  or atomic As. Further heating to 600 °C shows no additional As desorption. Figure 2 shows that one can use desorption techniques to control the surface stoichiometry of the As/GaAs(100). In particular, the difference in desorption temperatures between the second and third desorption peaks is large enough to allow us to resolve two different surface stoichiometries of GaAs(100) by incrementally desorbing the surface As. We used three desorption steps consisting of heating the As/MBE-grown GaAs(100) system for 10 s at 450, 530, and 570 °C. After each desorption step we carried out Auger electron spectroscopy (AES), CLS, and PLS measurements. Auger spectra showed an increase in the ratio  $R_s = \text{Ga}[MNN, 55\text{eV}]/\text{As}[MNN, 91\text{eV}]$  (surface-sensitive Auger) after each heating step. The quantitative analysis of the AES results involves a large error because of the large change in slope of the Auger spectrum base line due to variation in electron multiplier gain with electron energy. Nevertheless, the relative change in  $R_s$  is  $\sim 12\%$  between the first and second heating step but only a small change between the second and third step.

The CLS results show that changes in the optical emission spectrum occur after each heating step. Figure 3 depicts CL spectra after heating the As/GaAs(100) ( $n = 2 \times 10^{16} \text{ cm}^{-3}$ ) system for 10 s at several temperatures. The bottom spectrum shows that heating up to 450 °C causes a large re-

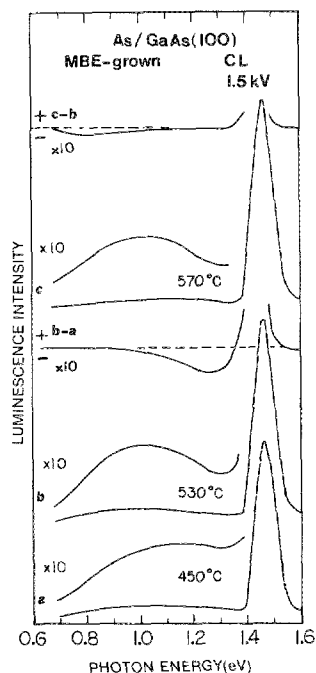


FIG. 3. CL spectra of As/MBE-grown GaAs(100) after heating for 10 s at indicated temperatures.

duction in the optical emission from the 0.8 eV shoulder and an increase in NBG transition intensity. Subsequent heating at 530 °C causes a diminution in the intensity of emission at about 1.25 eV, as shown in the difference spectrum  $b - a$ , and a small increase in NBG intensity. Raising the specimen temperature to 570 °C produces a further reduction in the 0.8 eV emission intensity and increase in NBG intensity. The difference spectra  $c - b$  shows this additional change. The CL spectra depicted in Fig. 3 show two emissions at 0.8 and 1.25 eV which are related to the As content and surface structure of MBE-grown GaAs(100).

## B. Metal-induced interface states

Figure 4 depicts CL spectra of clean and Au-covered MBE-grown GaAs(100) ( $n = 5 \times 10^{16} \text{ cm}^{-3}$ ). The spectra show that deposition of Au on clean MBE-GaAs(100) reintroduces interface states at energies 0.8 and 1.25 eV, and causes a large decrease in the NBG transition intensity. This reduction is due to increased SRV and band bending caused by the Au deposition, which moves  $E_f$  to 0.2 eV above the VB maximum (VBM) from the  $E_f$  midgap position of clean MBE-GaAs(100).<sup>9</sup> The NBG intensity measured by PLS also shows a large reduction, consistent with increased band bending.

Figure 5 depicts the CL spectra of the clean and Al-covered MBE-grown GaAs(100) ( $n = 2 \times 10^{16} \text{ cm}^{-3}$ ). Deposition of Al on clean GaAs causes the formation of two new emissions at 0.8 and 1.25 eV, and reduction on the overall luminescence intensity. This reduction is probably caused by an increase in SRV. Depth resolved CLS shows a small positive change in the NBG/deep level intensity ratio with Al deposition. This result agrees with SXPS experiments which

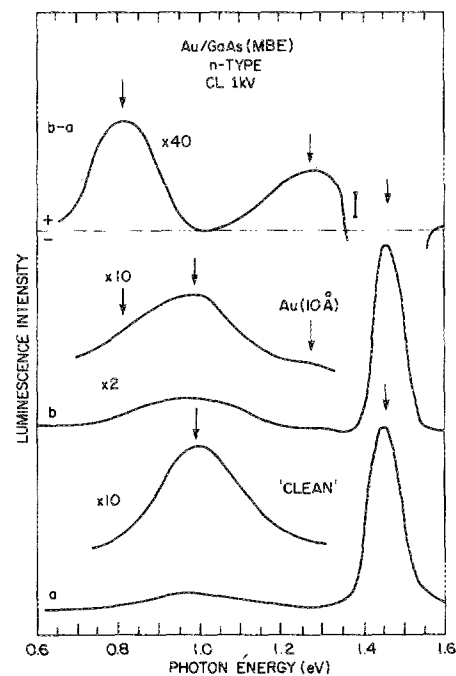


FIG. 4. CL spectra of clean and Au deposited MBE-grown GaAs(100). The vertical bar in the difference spectra indicates the noise level.

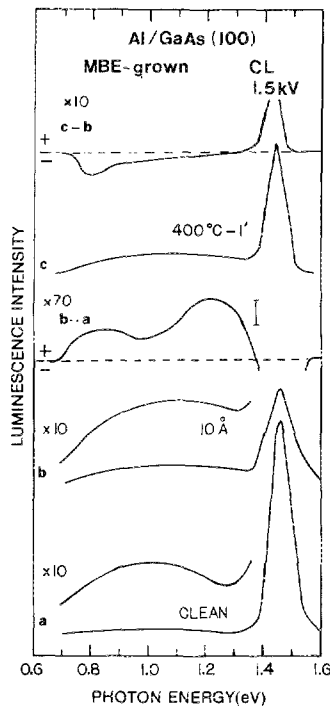


FIG. 5. CL spectra of clean and Al-deposited MBE-grown GaAs(100), and subsequent annealing to 400 °C for 1 min. The vertical bar in the difference spectra indicates the noise level.

show diminished band bending,  $\sim 0.2$  eV, upon Al deposition.<sup>19</sup> These peak energies are quite close to those of the Au/GaAs system; however, their intensity ratio is different. For Au/MBE-GaAs interfaces the emission intensity ratio  $RI[0.8 \text{ eV}/1.25 \text{ eV}]$  is  $\sim 1.8$ , whereas for Al/MBE-GaAs interfaces, this ratio is  $\sim 0.5$ . SXPS measurements of this system showed that the final  $E_f$  stabilization energy is 0.8–0.9 eV above VBM.<sup>9</sup> For Au/MBE-grown GaAs(100),  $E_f$  lies 0.2 eV above VBM. The ratio increase from Al to Au could be due to the  $E_f$  shift from above midgap to below midgap, thereby depopulating midgap states and increasing the transition probabilities for luminescent transitions from the conduction band. On the other hand, if the cross sections for radiative recombination of these discrete interface states do not depend on band bending, then Fig. 5 shows that the concentration of metal-induced interface states at a given energy depends upon the particular metal.

The lower  $RI[0.8 \text{ eV}/1.25 \text{ eV}]$  for Al/MBE-grown GaAs interfaces can be interpreted as due to the reduction of As at the Al/GaAs interface caused by reaction with metallic Al. Figure 5 shows that annealing of this junction at 400 °C for 1 min causes further reduction in the intensity of the 0.8 eV emission and increases the NBG emission intensity, indicating a reduction in band bending and SRV. This additional change in the spectral intensity supports our assumption that the 0.8 eV emission is linked to the presence of As at the interface. Indeed, SXPS experiments of this system show that the amount of bonded Al increases after heating.

Figure 6 depicts the CL spectra of liquid-encapsulated Czochralski (LEC)-grown GaAs(110) after cleavage and subsequent Al deposition. The bottom spectrum shows CLS of the freshly cleaved (110) surface. We notice that the optical emission from deep levels is much larger than that from MBE-grown material. Low-temperature PLS of both mate-

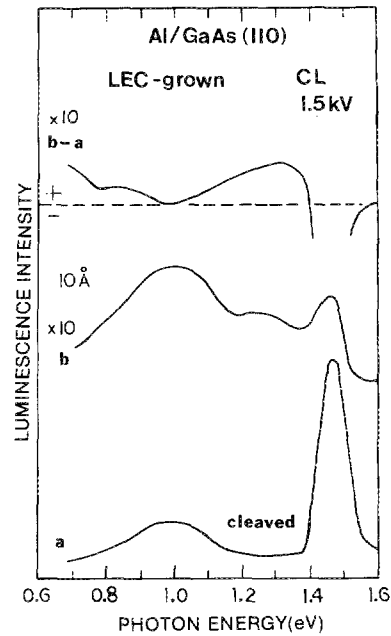


FIG. 6. CL spectra of UHV cleaned and Al deposited LEC-grown GaAs(110).

rials shows that emission from deep levels is at least two orders of magnitude larger for melt-grown GaAs.<sup>19</sup> For the melt-grown GaAs, the relatively high intensity of the NBG transition is due to the flat-band condition of the cleaved (110) surface. Deposition of Al causes a large reduction of NBG transition intensity, a broadening of the deep level band to lower energies, and the formation of a new emission at about 1.25 eV. The difference spectrum on the top of the figure shows that there is detectable emission at energies below 0.75 eV. This emission was not present in metal/MBE-grown GaAs interfaces.

A more dramatic picture is observed in the CL spectra of the Au/LEC-grown GaAs(110) system. Figure 7 depicts CL spectra of LEC-grown GaAs(110) after cleavage and subsequent Au deposition. At multilayer metal coverages, a

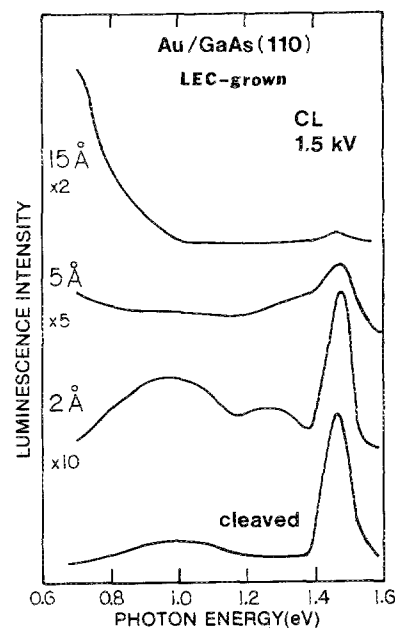


FIG. 7. CL spectra of UHV cleaned and Au deposited LEC-grown GaAs(110).

very intense optical emission develops and dominates the spectral shape. This emission and the associated interface state represent the major difference between the CLS features of Au on the melt-versus MBE-grown GaAs surfaces.

#### IV. DISCUSSION

##### A. TDS, surface stoichiometry and structure, and As-related states

The TDS and CLS experiments provide a clear picture of the different desorption stages and discrete surface states associated with the surface stoichiometry and reconstruction of the GaAs(100) surfaces. We have not yet performed LEED measurements as a function of As desorption. However, we have determined that heating below 400 °C produces a  $1 \times 1$  LEED pattern, a result obtained for As-rich surfaces by others.<sup>10–12</sup> However, LEED and scanning tunneling microscopy (STM) measurements carried out on similar MBE-grown GaAs(100) (same IBM source) and using similar thermal treatments for As decapping showed that there are primarily two reconstructions associated with the thermal processes reported above.<sup>13</sup> Heating up to 450 °C seems to form a  $(4 \times 2)$  reconstruction, subsequent heating to 550 °C changes the reconstruction to  $(2 \times 4)$ . These reconstructions coincide with a decrease in the surface As composition. The stoichiometry ratio  $R_s$  for these GaAs(100) surfaces decreases from  $\sim 0.72$  to  $\sim 0.98$  with increased temperature for our equivalent surfaces. From Fig. 7, the two main transitions at 0.8 and 1.25 eV associated to these reconstructed surfaces exhibit a strong dependence on  $R_s$ . Heating the specimen to 450 °C reduces the 0.8 eV emission intensity while changing the 1.25 eV emission intensity very little. Heating to 530 °C produces further desorption of As and changes the intensity of the 1.25 eV emission. In contrast, SXPS measurements on these surfaces show that  $E_f$  exhibits only minor changes with this modification on  $R_s$ . Hence the changes in stoichiometry and reconstruction appear to be directly related to the densities of electronic states at the GaAs surface.

##### B. CLS and PLS of clean MBE-versus melt-grown GaAs

The CLS and PLS measurements reported here show that both MBE- and melt-grown GaAs exhibit emission from states deep within the band gap. However, both the interface and bulk states for melt-grown GaAs exhibit emission which is much more intense than for MBE-grown GaAs. For melt-grown GaAs, the deep level concentrations appear to be over two orders of magnitude larger than those of MBE-grown GaAs. These may be related to a relatively large density of bulk trap states which occur in the melt-grown material.<sup>14,15</sup> The density and nature of these bulk traps depends on the growth method and is known to be relatively low for MBE-grown material.<sup>16</sup> Thus the interface state energies and densities appear to be strongly influenced by the quality of the near-surface region, due either to the method of growth and/or thermal post-treatment.

##### C. CLS of metal/GaAs interfaces: Similarities and differences

Metal deposition on clean GaAs surfaces causes drastic changes in the relative optical emission intensities and spectral shape, due both to band bending and the formation of interface states. The energies of the emission induced for both Au and Al on MBE-grown GaAs are similar. However, two metals produce over a factor of 3 difference in the relative intensities of the 0.8 vs 1.25 eV emissions. Whether or not these emission intensities reflect differences in state densities depends on how sensitive the luminescence transition cross sections are on the  $E_f$  position. For example, the reduced  $RI[0.8 \text{ eV}/1.25 \text{ eV}]$  for Al/GaAs interfaces can be interpreted as due to the reduction of As at the interface caused by the reaction with Al. Moreover, annealing this junction of 400 °C for 1 min further reduces the intensity of the 0.8 eV emission and increases the near band gap emission intensity, consistent with a further reduction of As. On the other hand, Al deposition and subsequent annealing both decrease the band bending, moving  $E_f$  toward the conduction band and possibly increasing the cross section for conduction band-midgap transitions. CLS measurements of other metals on MBE-grown GaAs may resolve this point. Overall, the similarities between the optical emission of As- and metal-covered interfaces on MBE-grown GaAs strongly suggest that the states involved have a similar origin, and that they are in fact related to excess As at the interface.

The discrete states produced by metal deposition also depend strongly on the nature of the GaAs substrate itself. For melt-grown GaAs, the energies of the optical emissions at low-metal coverage are similar to those of metal/MBE GaAs. However, with increasing metal coverages an intense emission develops at energies  $< 0.75 \text{ eV}$  and dominates the spectral shape at multilayer coverages. This emission, absent at metal/MBE-grown GaAs interfaces, may well be related to the large concentration of deep levels present in the LEC-grown GaAs, and strongly suggests the role of the associated states in determining the different barrier properties found at metal/LEC-GaAs interfaces. In this sense, the features at 0.8 and 1.25 eV could support a Schottky barrier model based on native defects. However, such a model must apparently depend strongly on the quality of the semiconductor material. Furthermore, such a model does not account for the wide continuous range of  $E_f$  positions observed in SXPS<sup>19</sup> (see also next section).

##### D. Schottky barrier and interface states

The direct observation of discrete GaAs interface states and their dependence on surface preparation, metallization, and bulk material have significant consequences for several models of Schottky barrier formation. First of all, the discrete states produced by metal deposition at energies close to the position at which  $E_f$  pins in melt-grown GaAs is contrary to a metal-induced gap state (MIGS) model<sup>17,18</sup> in which the intrinsic band structure of the semiconductor rather than any extrinsic states produced by interface formation defines the  $E_f$  position. In such a MIGS model, one expects a minimum rather than a maximum in the density of any interface states at the  $E_f$  stabilization energy. The wide

range of  $E_f$  stabilization energies now seen for MBE-grown GaAs<sup>19</sup> as well as other semiconductors<sup>8,20</sup> also argues against such models. Similarly, the dependence of the interface state energies and densities on surface preparation, metallization, and substrate material argues against defect models in which the energies and densities of interface states for a given semiconductor are constant, regardless of the adsorbate.<sup>21</sup> Instead the orders-of-magnitude lower interface state density and different energies for the deep levels in MBE-grown GaAs versus melt-grown GaAs are consistent with the much wider range of  $E_f$  stabilization energies.<sup>19</sup> Interface defects may play a role in Schottky barrier formation, but the CLS results presented here show that their energies and densities depend on the quality of the semiconductor substrate, as determined by the growth method and/or subsequent thermal treatments.

The differences between Au and Al/GaAs interface emission also suggests that interface chemistry can affect the nature of such defects strongly. The strong dependence of interface state features on As chemistry lends strong support to the central role of excess As at the metal/GaAs interface.<sup>22</sup> Such excess As can produce an interfacial phase with a relatively constant work function, independent of the metallization.<sup>22</sup> Alternatively, excess As leads to formation of  $As_{Ga}$  antisite defects which can produce deep levels near the  $E_f$  pinning positions in melt-grown GaAs.<sup>23</sup> Experiments are in progress to distinguish between these two alternatives.

Finally, the lower density of interface states evident for the MBE-grown GaAs permits us to view such states as a perturbation on a self-consistent electrostatic model for charge transfer and band bending at the metal/GaAs interface.<sup>24</sup> Significantly, the 1.25 eV CLS transition observed for the metallized surfaces corresponds closely to the low-density acceptor level 1.2 eV below the conduction band which is required to fit the dependence of barrier height to metal work function.<sup>19</sup> This energy found for the discrete states at metal/MBE-GaAs interfaces integrated within a Schottky formalism is thus capable of providing self-consistent results for the interface electrostatics.

## V. CONCLUSIONS

We have used CLS and PLS techniques to obtain a direct measure of the discrete electronic states at metal/GaAs interfaces. These states depend sensitively on the surface preparation, metallization, as well as the semiconductor material itself. The detailed evolution of optical emission energies and intensities with multilayer metal deposition are correlated to metal-induced states and  $E_f$  movements. The energy of the discrete states found at metal/MBE-grown GaAs(100) interfaces integrated within a Schottky formalism is capable of providing self-consistent results for the interface electrostatics. On the other hand, the presence of large concentration of extrinsic defects (i.e., due to native defect segregation from the bulk, chemical reaction, or interdiffusion) causes the pinning behavior observed at metal/melt-grown GaAs(110) interfaces. Our experimental observations, together with the analysis of the junction electrostatics provide

an internally consistent set of results supporting the conclusion that atomic (rather than electronic) relaxations at metal semiconductor interfaces is responsible for the insensitivity of the Schottky barrier height on metal work function observed on LEC materials. Our results provide the first direct experimental evidence for the origin of Fermi level pinning at metal/melt-grown GaAs junctions.

## ACKNOWLEDGMENTS

Partial support by the Office of Naval Research (Grant No. ONR N00014-80-C-0778) and fruitful discussions with Christian Mailhlot are gratefully acknowledged.

- <sup>1</sup>L. J. Brillson, Surf. Sci. Rep. 2, 123 (1982), and references therein.
- <sup>2</sup>G. Margaritondo, Solid-State Electron. 26, 499 (1988).
- <sup>3</sup>W. E. Spicer and S. J. Eglash, in *VLSI Electronics; Microstructure Science* (Academic, New York, 1985), Vol. 10, p. 79.
- <sup>4</sup>L. J. Brillson, H. W. Richter, M. L. Slade, B. A. Weinstein, and H. Shapira, J. Vac. Sci. Technol. A 3, 1011 (1985).
- <sup>5</sup>R. E. Viturro, M. L. Slade, and L. J. Brillson, Phys. Rev. Lett. 57, 487 (1986).
- <sup>6</sup>L. J. Brillson and R. E. Viturro, Scanning Microsc. 2, 789 (1988).
- <sup>7</sup>R. E. Viturro, J. L. Shaw, and L. J. Brillson, J. Vac. Sci. Technol. B 5, 1125 (1987).
- <sup>8</sup>L. J. Brillson, M. L. Slade, R. E. Viturro, M. Kelly, N. Tache, G. Margaritondo, J. M. Woodall, G. D. Pettit, P. D. Kirchner, and S. L. Wright, Appl. Phys. Lett. 48, 1458 (1986); J. Vac. Sci. Technol. B 4, 919 (1986).
- <sup>9</sup>R. E. Viturro, L. J. Brillson, J. L. Shaw, N. Tache, J. McKinley, G. Margaritondo, J. Woodall, P. D. Kirchner, G. D. Pettit, and S. L. Wright (unpublished).
- <sup>10</sup>R. Z. Bachrach, R. S. Bauer, P. Chiaradia, and G. V. Hansson, J. Vac. Sci. Technol. 19, 335 (1983).
- <sup>11</sup>W. I. Wang, J. Vac. Sci. Technol. B 1, 574 (1983).
- <sup>12</sup>S. P. Svensson, J. Kanski, T. G. Andersson, and P.-O. Nilsson, J. Vac. Sci. Technol. B 2, 235 (1984).
- <sup>13</sup>M. D. Pashley, K. W. Haberern, and J. M. Woodall, J. Vac. Sci. Technol. B 6, 1468 (1988).
- <sup>14</sup>D. E. Holmes, R. Y. Chen, K. R. Elliot, and C. G. Kirkpatrick, Appl. Phys. Lett. 40, 46 (1982).
- <sup>15</sup>J. Lagowski, H. C. Gatos, J. M. Parsey, K. Wada, M. Kaminska, and W. Walukiewicz, Appl. Phys. Lett. 40, 342 (1982).
- <sup>16</sup>A. Mirceau and D. Bois, Inst. Phys. Conf. Ser. 46, 82 (1979).
- <sup>17</sup>J. Tersoff, Phys. Rev. B 32, 6968 (1985).
- <sup>18</sup>W. Monch, Phys. Rev. Lett. 58, 1360 (1987).
- <sup>19</sup>R. E. Viturro, J. L. Shaw, C. Mailhlot, L. J. Brillson, N. Tache, J. McKinley, G. Margaritondo, J. M. Woodall, P. D. Kirchner, G. D. Pettit, and S. L. Wright, Appl. Phys. Lett. 52, 2052 (1988); L. J. Brillson, R. E. Viturro, C. Mailhlot, J. L. Shaw, N. Tache, J. McKinley, G. Margaritondo, J. M. Woodall, P. D. Kirchner, G. D. Pettit, and S. L. Wright, J. Vac. Sci. Technol. B 6, 1263 (1988).
- <sup>20</sup>L. J. Brillson, R. E. Viturro, M. L. Slade, P. Chiaradia, D. Kilday, M. Kelly, and G. Margaritondo, Appl. Phys. Lett. 50, 1379 (1987); P. Chiaradia, L. J. Brillson, R. E. Viturro, M. L. Slade, D. L. Kilday, M. Kelly, and G. Margaritondo, J. Vac. Sci. Technol. B 5, 1075 (1987).
- <sup>21</sup>W. E. Spicer, I. Lindau, P. Skeath, and C. Y. Su, J. Vac. Sci. Technol. 16, 1418 (1980).
- <sup>22</sup>J. M. Woodall and J. L. Freouf, J. Vac. Sci. Technol. 19, 794 (1981); J. L. Freouf and J. M. Woodall, Appl. Phys. Lett. 39, 727 (1981).
- <sup>23</sup>W. E. Spicer, T. Kendelewicz, N. Newman, R. Cao, C. McCants, K. Miyano, I. Lindau, and E. R. Weber, J. Vac. Sci. Technol. B 6, 1245 (1988).
- <sup>24</sup>C. B. Duke and C. Mailhlot, J. Vac. Sci. Technol. B 3, 1970 (1985); C. Mailhlot and C. B. Duke, Phys. Rev. B 33, 1118 (1986).